Effect of Inclination on the Performance of a Compact Brazed Plate Condenser and Evaporator

MARK A. KEDZIERSKI

National Institute of Standards and Technology, Building and Fire Research Laboratory, Gaithersburg, Maryland, USA

This study experimentally quantified the change in heat transfer and pressure drop associated with tilting a compact brazed plate heat exchanger from the intended vertical position. Both clockwise and counterclockwise rotations within a plane perpendicular to the fittings were examined. A SWEP B15 × 36 was tested as an R-22 evaporator and condenser under fixed refrigerant state conditions suitable to high-efficiency water-source heat pumps. This study showed that a substantial performance penalty occurred when the evaporator was rotated past 30° from the vertical. The evaporator heat transfer in the horizontal position was 60–75% of the vertical value. For a rotation angle of 30°, the degraded heat transfer was within 5% of the vertical value. Rotation direction and entering refrigerant state had little effect on the performance of the evaporator for rotation angles less than 60°. Only when the evaporator was rotated to the horizontal position did rotation direction and refrigerant state have much effect. At the horizontal position, a subcooled-entering refrigerant and a counterclockwise rotation both tended to lessen the evaporator heat transfer degradation. Rotation of the condenser to the horizontal position improved the overall heat transfer coefficient by approximately 17–30%. Rotation direction had a negligible effect on the performance of the condenser for angles less than 60°. Both the evaporator and condenser pressure drops were influenced by flow distribution changes as the heat exchangers were rotated.

The origins of the compact brazed plate heat exchanger (CBE) began in the 1920s with the first commercially successful gasketed-plate heat exchangers (Saunders [1]). Milk producers and other food and drink processors satisfied hygiene requirements by periodically disassembling and cleaning the gasketed plates. The convenience of disassemblage limits the application of gasketed-plate heat exchangers to relative low-pressure duties. By contrast, the CBE can sustain relatively large operating pressures because the edges of its plates are brazed together.

Applications for compact brazed plate heat exchangers have increased in recent years. Currently, the compactness of the CBE drives its use as refrigerant evaporators and condensers. For example, Saunders [1] cites a case where one CBE replaced several shell-and-tube heat exchangers. Consequently, research demonstrating the use of CBEs in refrigeration applications, such as that of Falls et al. [2] and Jonsson [3], is becoming more prevalent. The accelerated application of CBEs to

Received 20 March 1996; accepted 1 April 1997.

NIST and The Trane Company, under Project Manager Gary Lange, funded this work jointly. Thanks go to the following NIST and Trane personnel for their constructive criticism of the first draft of the manuscript: Dr. D. Didion, Mr. B. Dougherty, Mrs. J. Land, and Mr. G. Lange (Trane). The author would also like to express appreciation to Mr. A. Goelz and Mr. J. Sponsky for data collection.

Address correspondence to Dr. Mark A. Kedzierski, Thermal Machinery Group, Building 226, Room B114, National Institute of Standards and Technology, U.S. Department of Commerce, Gaithersburg, MD 20899-0001, USA. E-mail: squid@nist.gov

refrigerant equipment is sustained by pertinent design information. Unfortunately, the available research on CBEs as refrigerant evaporators and condensers is not entirely comprehensive.

No work was found in the open literature on the influence of gravity on the heat transfer performance of a CBE. Much of the work toward developing the means to predict the duty of plate heat exchangers has focused on single-phase heat transfer [4–6], where gravity effects should be insignificant. Also, two-phase studies with CBEs, such as that by Wang and Zhao [7], remove the gravity effect by assuming a vertical installation. Intuitively, gravity should significantly affect the flow patterns in the narrow channels of a CBE. Consequently, tilting a CBE should affect the two-phase heat transfer.

The purpose of this study was to quantify the change in performance associated with tilting a CBE from the designed vertical position. It may be advantageous to install the CBE skewed in equipment to achieve a lower-profile, and consequently, lower-cost unit enclosure. A manufacturer may be willing to give up a certain heat exchanger duty to be able to produce less expensive equipment. Accordingly, detailed measurements of the effect of inclination on the performance of a CBE are required to carefully weigh the performance change against the production cost savings. Also, manufacturers of CBEs can provide their customers with performance-versus-orientation design information that may create new applications for CBEs or increase the use of CBEs in existing applications. For example, this study shows that the heat transfer performance of an R22 CBE condenser in the horizontal position is greater than in the vertical position. This result may encourage the use of CBEs in more condenser applications.

A SWEP B15 × 36 was tested under operating conditions experienced by an evaporator and a condenser of a high-efficiency water-source heat pump. The B15 × 36 contained thirty-six 466 mm × 72 mm stainless steel plates with a ridged herringbone pattern. The plates were stacked alternating the orientation of the herringbone pattern and then brazed with copper. The honeycomb pattern the stacked plates create is illustrated in the cutaway drawing of a typical CBE given in Figure 1. When viewed in the vertical position, the CBE had 19-mm NPT connections located on the right front for the water stream and 22-mm solder connections on the left front for the refrigerant stream.

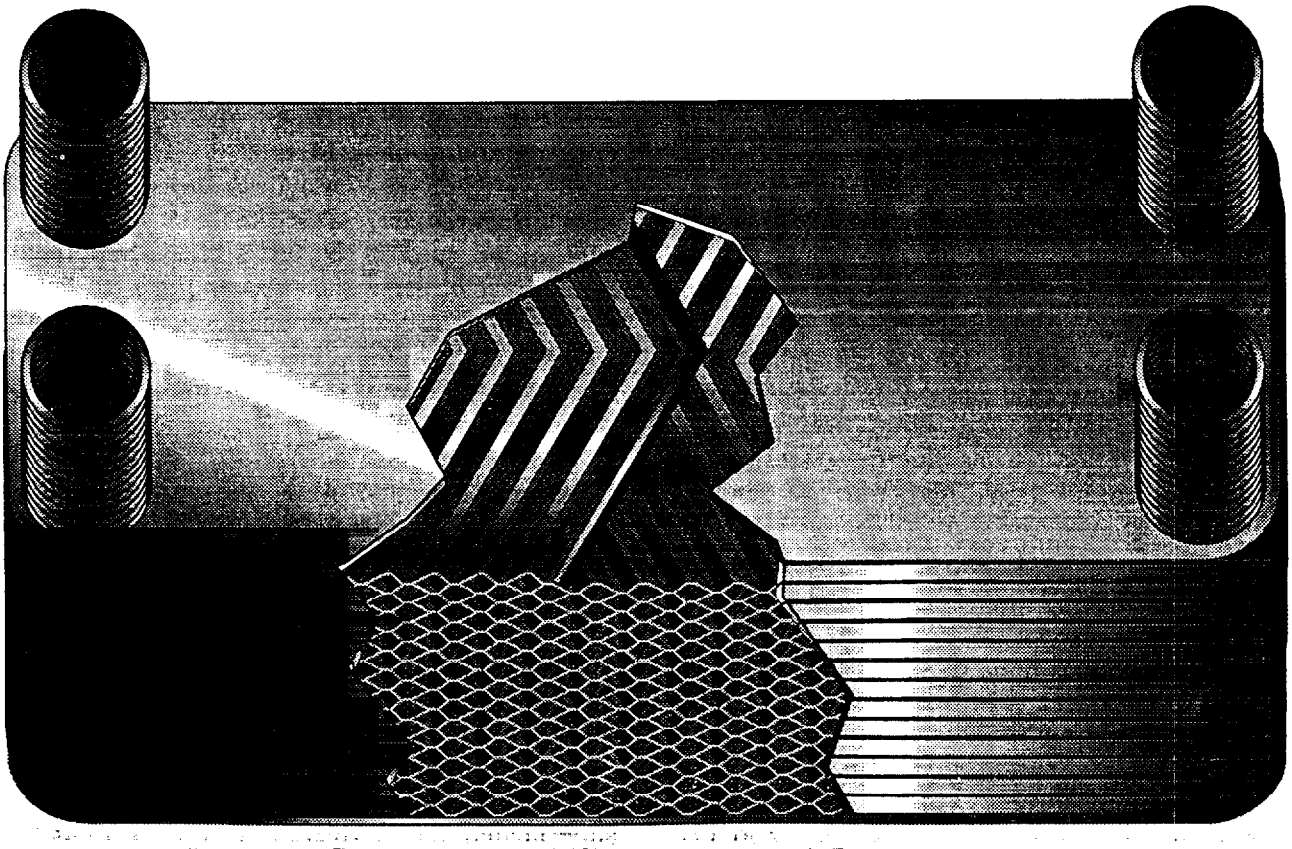

Figure 1 Cutaway of typical compact brazed plate heat exchanger.

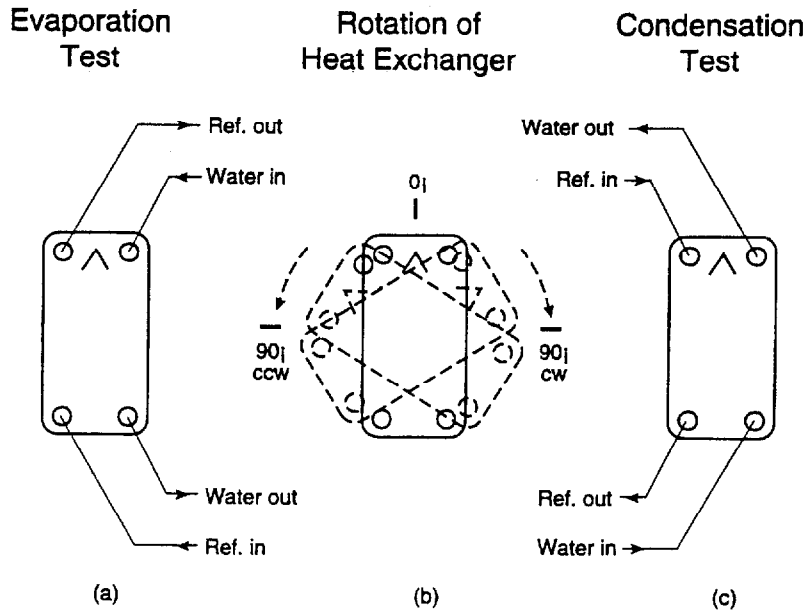

Figure 2 Test heat exchanger orientation.

Figure 2 illustrates the orientation of the test heat exchanger as it was rotated clockwise and counterclockwise about an axis perpendicular to and centered on the front of the heat exchanger. Brazed plate heat exchangers have pointers stamped on the surface at one end, which manufacturers recommend to point upward when installed SWEP [8]. Figures 2*a* and 2*c* show the evaporator and the condenser in the recommended vertical orientation, respectively. The fluid connections were located at the corners of the heat exchanger and extended outward from its face. The fluid streams of both the evaporator and the condenser were in counterflow. The refrigerant flowed up in the evaporator and down in the condenser. The heat exchanger was rotated about an axis centered on its face and parallel to the axis of the connections. The angle of rotation was measured from the vertical position. Both rotation directions were tested to examine the effect of the position of the connections relative to the header.

TEST APPARATUS

Figure 3 shows a schematic of the test rig used to test the brazed plate heat exchanger. The main components of the rig are labeled on the figure as (1) subcooler, (2) refrigerant pump, (3) desubcooler, (4) preevaporator, (5) reservoir/liquid desuperheater, (6) test heat exchanger, and (7) condensers. The de-subcooler was bypassed during the evaporation tests. The different refrigerant paths for evaporator and condenser tests are illustrated in Figure 3.

The desubcooler was operated and the desuperheater was disabled during the condensation tests. The purpose of the desubcooler was to remove the subcooling. The subcooling prevented cavitation in the pump. The phase change occurred in the preevaporator, where the saturation pressure was more readily controlled when the evaporator had little subcooling to remove. The refrigerant charge was reduced enough to keep liquid out of the desuperheater. Otherwise, saturated liquid would have entered the test section. Superheated vapor traveled from the preevaporator to the test condenser. The test condenser condensed the refrigerant, which then bypassed the brine-cooled condensers and traveled to the subcooler to complete the loop.

The desubcooler was bypassed and the desuperheater was operated during the evaporation tests. For the evaporator tests, the refrigerant exited the preevaporator as saturated liquid at approximately 1% thermodynamic quality. The low-quality liquid–vapor mixture entered the top of the liquid desuperheater and exited the bottom as saturated liquid. The system charge was adjusted to keep liquid refrigerant in the bottom of the desuperheater. The refrigerant leaving the desuperheater entered the test evaporator. The test evaporator superheated the refrigerant to approximately 5.5 K above the saturation temperature. The refriger-

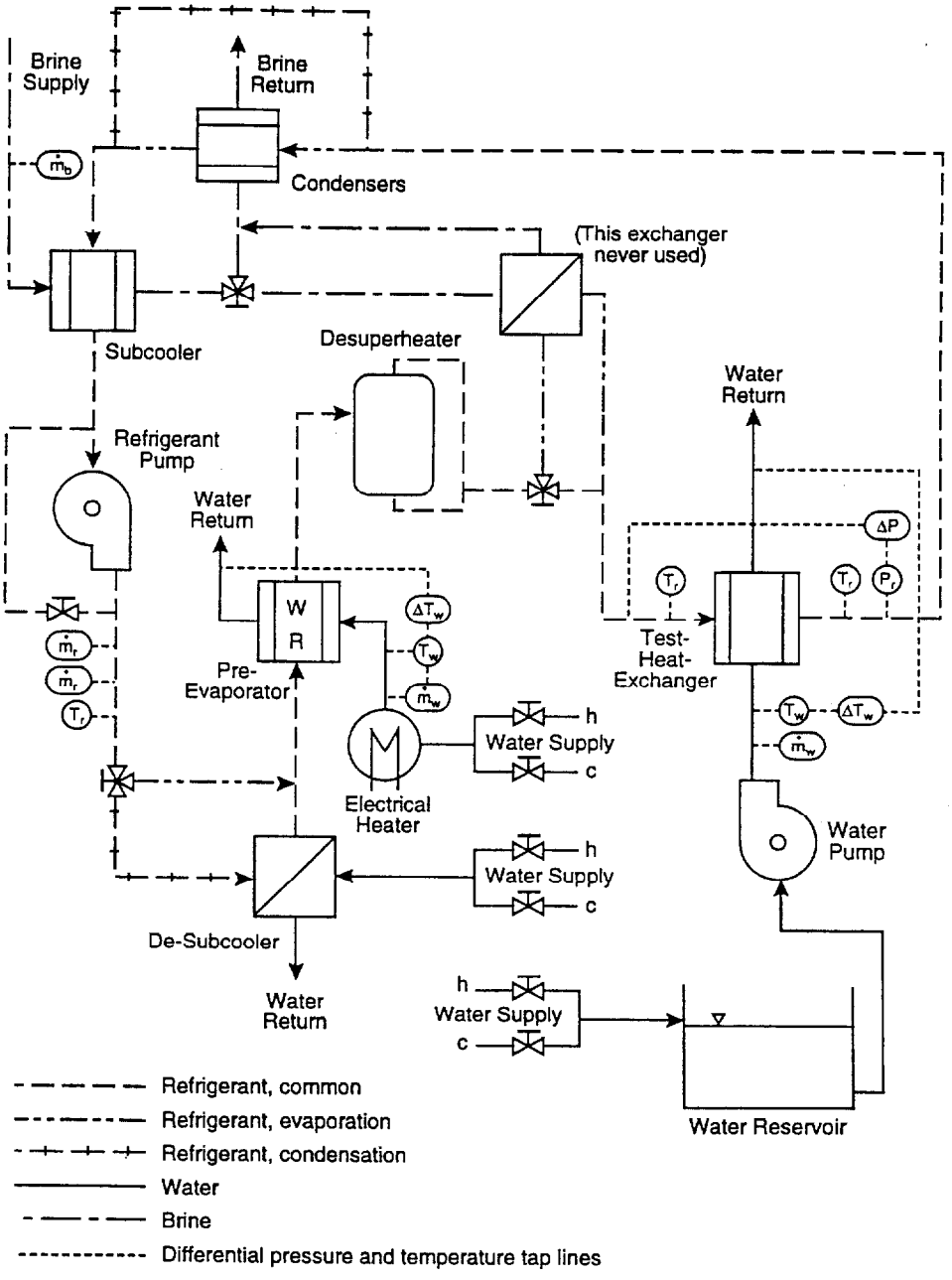

Figure 3 Schematic of the test rig.

ant circuit was completed by the condensation of the superheated vapor in the condensers.

The loop contained all brazed plate heat exchangers except for the brine-cooled condensers, which were aluminum spiral heat exchangers. Brine at 260 K and 0.24 kg/s subcooled and condensed the test refrigerant in the subcooler and condensers, respectively. The mass flow rate of the subcooled refrigerant measured with the coriolis meter and that measured with the turbine meter always agreed within 1%.

Figure 3 illustrates the location of all the measurement devices. The subcooled liquid refrigerant temperatures were measured at the turbine meter and in the line between the desubcooler and the preevaporator. The refrigerant pressure was also measured in the line between the desubcooler and the preevaporator to determine the degree of subcooling there. The refrigerant temperatures were also measured in line at the entrance and exit of the test heat exchanger, along with the pressure drop across its inlet and exit. The absolute pressure of the refrigerant was measured at the inlet of the test heat exchanger.

Ten-element thermopiles were used to measure the water temperature drop of the test heat ex-

changer and the preevaporator. The separate water flow rates for the test heat exchanger and the preevaporator were measured with turbine meters to calculate the duty of each. The heat load of the preevaporator was used to calculate the inlet quality of the test heat exchanger. The heat load of the test heat exchanger was the focal point of this study and was also used to calculate its exit quality.

The duty of the test heat exchanger, the measured refrigerant temperatures, and saturation pressure were used to calculate the average temperature difference between the water and refrigerant streams ($\Delta\bar{T}$) of the test heat exchanger as

$$\frac{1}{\Delta\bar{T}} = \frac{q_v}{q_T\,\Delta T_v} + \frac{q_{2\phi}}{q_T\,\Delta T_{2\phi}} + \frac{q_l}{q_T\,\Delta T_l} \tag{1}$$

where the equations used to calculate the average temperature difference between the water and refrigerant vapor (ΔT_v), water and two-phase refrigerant ($\Delta T_{2\phi}$), and water and refrigerant liquid (ΔT_l) are given in Appendix A. Appendix B provides the equations used to calculate the vapor (q_v), two-phase ($q_{2\phi}$), and liquid (q_l) components of heat.

The overall conductance (UA) of the test heat exchanger was calculated as

$$UA = \frac{q_T}{\Delta\bar{T}} \tag{2}$$

The estimated combined standard uncertainty (u_c) of the UA calculation, along with all other measurement u_c's for 95% confidence, are presented in Table 1. The u_c is commonly referred to as the law of propagation of uncertainty.

Table 1 Combined standard measurement uncertainties

Measured parameter	u_c
Turbine ref. flow meter	±2% of the measured value
Coriolis ref. flow meter	± 10E-4 kg/s
Absolute temperature	0.2 K
Temperature difference	0.01 K
Absolute ref. pressure	±2 kPa
Differential pressure	±0.26 kPa
Duty test H-X	±2%
UA of test H-X	±4.3%
$\Delta\bar{T}$ (LMTD) of test H-X	±3.8%
ΔP of test H-X	0.2 kPa

The target operating conditions given in Tables 2 and 3 are applicable to those for current high-efficiency water-source heat pump evaporators and condensers, respectively. Due to the limitations of water and brine flow rates and temperatures of the test loop, certain target conditions were unattainable. Consequently, the "as tested" conditions are given in Tables 2 and 3. Most of the evaporator target conditions were met. The refrigerant flow rate was marginally lower than the target value. The saturation temperature for the evaporator test was approximately 10 K greater than the target value. The condenser was tested at a saturation pressure lower than the target condition. Also, the refrigerant mass flow rate of the condenser was approximately half that of the target, due to insufficient water flow to the condenser. It is believed that the observed relative performance with heat exchanger rotation should not be significantly different from that which would have been observed at the target conditions.

Table 2 Vertical evaporator operating conditions

Operating condition	Target	As tested, saturated inlet	As tested, subcooled inlet
Refrigerant flow rate in vertical position	0.055 kg/s (433 lb_m/h)	0.051 kg/s (402 lb_m/h)	0.051 kg/s (402 lb_m/h)
Refrigerant inlet temperature	280.37 K (45.0°F)	290.7 K (63.59°F)	289.8 K (61.97°F)
Saturated two-phase	280.37 K (45.0°F)	291.0 K (64.13°F)	290.9 K (63.95°F)
Exit superheat	5.56 K (10°F)	5.54 K (9.97°F)	5.52 K (9.94°F)
Inlet water temperature	294.3 K (70°F)	303.6 K (86.81°F)	303.1 K (85.91°F)
Water flow rate	0.55 kg/s (8.75 gal/min)	0.25 kg/s (3.98 gal/min)	0.25 kg/s (3.98 gal/min)

Table 3 Vertical condenser operating conditions

Operating condition	Target	As tested (counterclockwise)	As tested (clockwise)
Refrigerant flow rate	0.06 kg/s (480 lb_m/h)	0.028 kg/s	0.029 kg/s
Saturated condensing	311.8 K (101.6°F)	291.7 K	294.8 K
Refrigerant inlet temperature	347.0 K (165°F)	347.7 K	349.6 K
Subcooled exiting refrigerant temperature	303.7 K (101.6°F)	284.6 K	284.2 K
Entering water temperature	302.59 K (85°F)	284.5 K	284.1 K
Exiting water temperature	308.2 K (95°F)	289.3 K	289.1 K
Water flow rate	0.55 kg/s (8.75 gal/min)	0.33 kg/s	0.33 kg/s

TEST RESULTS

The test results for the evaporator and the condenser are summarized in Tables 4 and 5, respectively. The tables provide the heat load, the overall conductance, the mean temperature difference, and the refrigerant flow rate averaged for each rotation angle. The R-22 saturation temperature, the inlet and exit thermodynamic state conditions of the refrigerant, the water flow rate, and the inlet water temperature were all fixed for both the condenser and evaporator tests.

Figures 4–11 present the data given in Tables 4 and 5 normalized by the data measured when the CBE was in the vertical position. The lines given in the graphs were obtained from a cubic regression on the rotation angle. Table 6 provides the magnitude of the average 95% confidence interval for the cubic regression. Following is a discussion of Figures 4–12.

Table 4 Averaged evaporator data

ω (deg)	q_e (W)	UA_e (W/K)	$\Delta\bar{T}_e$ (K)	ΔP_e (kPa)	$\dot{m}_r$ (kg/s)
Clockwise rotation, saturated inlet conditions					
0	10,272	1,433	7.2	7.8	0.051
30	9,971	1,208	8.1	7.1	0.050
45	9,263	1,031	9.1	6.1	0.046
60	8,609	839	10.4	5.0	0.043
90	6,379	486	13.3	2.9	0.033
Counterclockwise rotation, saturated inlet conditions					
0	10,225	1,418	7.1	8.0	0.051
30	10,019	1,257	7.8	7.6	0.050
45	9,286	1,077	8.9	6.7	0.046
60	8,691	873	10.3	5.8	0.043
90	6,742	520	13.0	3.6	0.036
Clockwise rotation, subcooled inlet conditions					
0	10,225	1,336	7.7	7.1	0.051
30	9,875	1,145	8.6	6.6	0.049
45	9,151	987	9.5	5.6	0.046
60	8,708	816	10.6	4.6	0.043
90	7,010	522	13.5	3.6	0.038
Counterclockwise rotation, subcooled inlet conditions					
0	10,251	1,342	7.6	7.3	0.051
30	9,883	1,162	8.5	6.7	0.050
60	8,749	813	10.8	5.3	0.044
90	7,556	564	13.4	4.0	0.038

Table 5 Averaged condenser data

ω (deg)	q_c (W)	UA_c (W/K)	$\Delta\bar{T}_c$ (K)	ΔP_c (kPa)	$\dot{m}_r$ (kg/s)
		Clockwise rotation			
0	7,092	826	8.5	5.2	0.029
20	7,111	863	8.2	5.2	0.029
30	7,115	891	8.0	5.2	0.029
45	7,083	941	7.6	5.3	0.029
60	7,108	994	7.2	5.3	0.029
75	7,089	1,045	6.8	5.3	0.029
90	7,070	1,088	6.5	5.4	0.029
		Counterclockwise rotation			
0	6,861	1,199	5.7	4.4	0.028
20	6,884	1,281	5.4	4.3	0.028
30	6,860	1,314	5.2	4.3	0.028
45	6,918	1,353	5.1	4.4	0.028
60	6,876	1,380	5.0	4.5	0.028
75	6,861	1,398	4.9	4.8	0.028
90	6,793	1,405	4.8	5.3	0.028

Evaporator

The test procedure for the evaporator was designed to simulate how an actual heat pump would react to a loss of evaporator heat transfer when the evaporator was tilted. The function of a thermostatic or electronic expansion valve in a heat pump is to adjust the refrigerant flow rate so that a desired superheat exits the evaporator. A loss of heat transfer causes the expansion valve to reduce the refrigerant flow rate to maintain a fixed evaporator superheat. Maintaining fixed exiting evaporator superheat while the evaporator heat transfer deteriorated was achieved by reducing the refrigerant pump speed in the present test loop.

Four different test sets were performed on the evaporator. The first two sets were for saturated entering refrigerant conditions; one test set was rotated clockwise, and the other test set was rotated counterclockwise. The last two test sets were for subcooled-entering refrigerant with the test heat exchanger rotated clockwise and counterclockwise. The subcooled-entering refrigerant tests were used to investigate the effect of flow distribution on the performance of the evaporator. Engelhorn and Reinhart [9] showed that flow maldistribution adversely affects the performance of an R-22 CBE evaporator. Also, Edwards et al. [10] have shown experimentally that maldistribution of single-phase flow is relatively insignificant

Table 6 Average magnitude of 95% confidence interval for mean given in graphs

Test	UA/UA_0	q/q_0	$\Delta T/\Delta T_0$	$\Delta P/\Delta P_0$	$\dot{m}/\dot{m}_0$
Evaporator cw, saturated inlet	0.021	0.014	0.026	0.04	0.013
Evaporator ccw, saturated inlet	0.022	0.020	0.031	0.05	0.018
Evaporator cw, subcooled inlet	0.031	0.015	0.048	0.07	0.008
Evaporator ccw, subcooled inlet	0.038	0.014	0.040	0.05	0.008
Condenser cw	0.059	0.004	0.041	0.01	n/a
Condenser ccw	0.080	0.003	0.046	0.02	n/a

for 20 plates. For a 40-plate CBE, Edwards et al. [10] found that the mass flow in the first 24 plates and the last 16 plates was on average 8% below and 8% above a uniformly distributed flow, respectively. The present CBE contains 36 plates. Consequently, if the saturated entering flow is maldistributed, the subcooled-entering flow should exhibit a more uniform flow distribution and a smaller performance degradation. The amount of subcooling was set equal to the drop in saturation temperature that would have occurred for the entire pressure drop of the test heat exchanger. This criterion lessened the amount of flashing that occurred at the entrance and possibly eliminated it.

Figure 4 shows the normalized duty of the evaporator as a function of inclination angle (ω). For a given test condition, the data were normalized by the duty measured at the vertical position (q_{e0}). The data illustrate that for rotation angles less than 60°, similar capacities were observed for clockwise, counterclockwise, saturated, and subcooled-entering conditions. For 30°, the evaporator heat transfer was within 5% of the vertical (0°) value. For angles greater than 30°, the heat transfer rapidly degraded. In the horizontal position (90°), the heat transfer was approximately 60–75% of the vertical position duty. The performance degradation in the horizontal position depended on the refrigerant entering state and the rotation direction. Both subcooled-entering refrigerant and a counterclockwise rotation tended to minimize the performance degradation. This suggests that neither refrigerant flow distribution nor the relative position of the refrigerant and water connection has much effect on heat transfer until the evaporator is nearly horizontal.

Figure 5 shows the refrigerant mass flow rate ($\dot{m}_e$) reduction required to maintain the 5.56 K (10°F) exit evaporator superheat. As expected, the heat transfer loss was directly proportional to the refrigerant mass flow rate reduction. The severe deterioration of the mass flow rate did not occur until the heat exchanger was tilted past 30°.

Figures 6 and 7 show the normalized overall conductance (UA_e) and the composite log-mean temperature difference ($\Delta\overline{T}_e$) versus inclination angle (ω). The rate of decrease of the UA_e (increase of the $\Delta\overline{T}_e$) for angles greater than 30° was marginally greater than the decrease of the UA_e (increase of the $\Delta\overline{T}_e$) for angles less than 30°. For 30°, the mean $\Delta\overline{T}_e$ remained within 15% of the vertical value. Neither rotation direction nor entering-refrigerant condition had much effect on the UA_e or the $\Delta\overline{T}_e$ for angles less than 60°. However, when the evaporator was in the horizontal position, both subcooled-entering refrigerant and a counterclockwise rotation tended to reduce UA_e and increase $\Delta\overline{T}_e$.

Figure 8 shows the refrigerant-side, evaporator pressure drop (ΔP_e) for refrigerant upflow plotted against the rotation angle. The mean pressure drop remained within 10% of the vertical value for a rotation angle of 30°. For rotation angles greater than 30°, the pressure drop decreased to approximately 35–55% of the vertical value at the horizontal position. Both the gravitational pressure drop and the frictional pressure drop diminish as the evaporator is rotated toward the horizontal position. Obviously, no gravitational

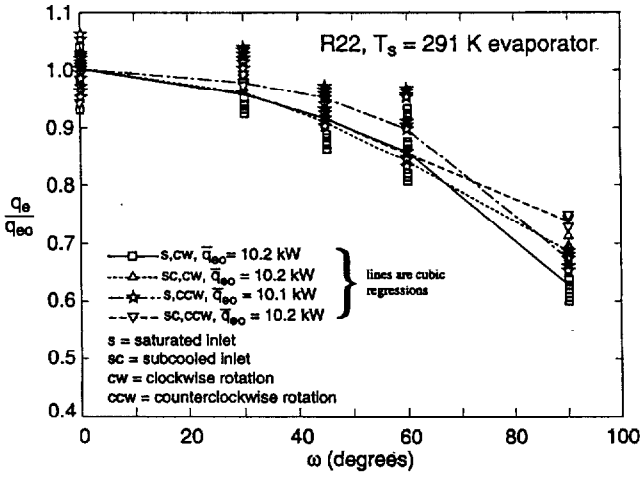

Figure 4 Normalized duty of the evaporator as a function of inclination angle.

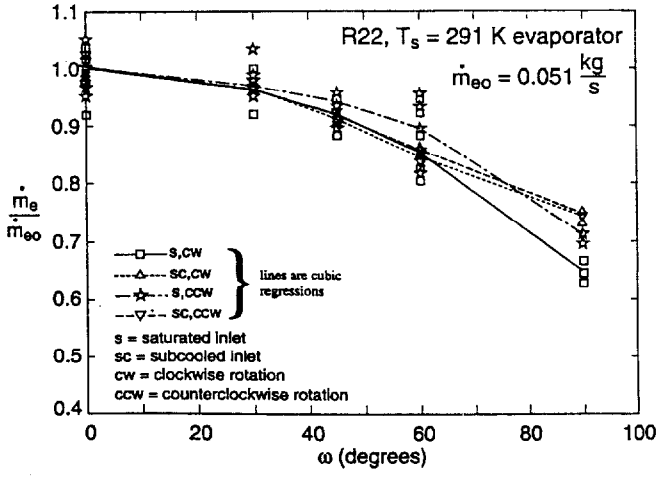

Figure 5 Refrigerant mass flow rate reduction required to maintain the 5.56 K (10°F) exit evaporator superheat.

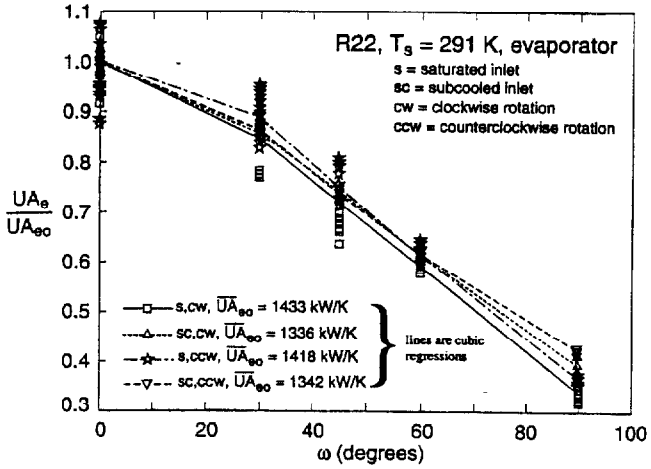

Figure 6 Overall evaporator conductance versus inclination angle.

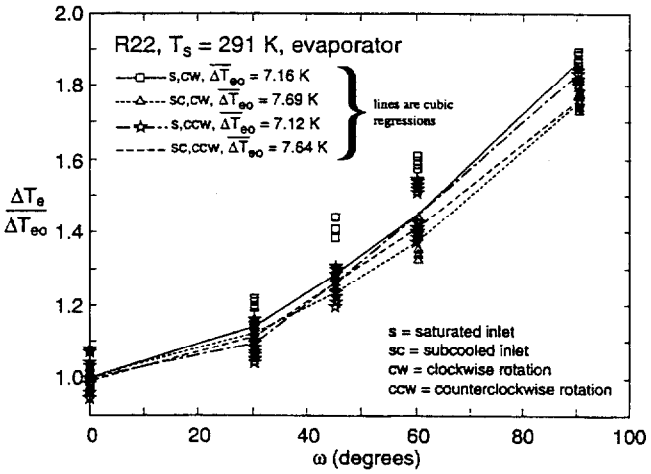

Figure 7 Composite log-mean temperature difference of evaporator versus inclination angle.

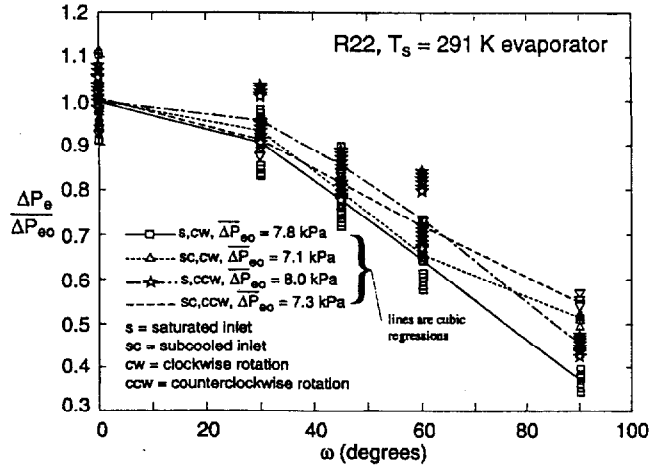

Figure 8 Refrigerant-side pressure drop of evaporator versus inclination angle.

pressure drop exists when the refrigerant flows horizontally. The reason for the reduction in the frictional pressure drop is not as obvious. The frictional pressure drop becomes smaller as the refrigerant flow changes from annular-like to stratified. Presumably, the refrigerant flow is well distributed throughout a vertically positioned compact brazed plate heat exchanger. By contrast, the refrigerant flow should be relatively stratified when the same heat exchanger is horizontal. A significantly larger portion of the heat transfer surface contacts the vapor phase for stratified flow than for a well-distributed flow. Consequently, the frictional pressure drop for stratified flow is smaller than that for a well-distributed, vertical flow.

In summary, the designer should heed the CBE manufacturers' recommendations for a vertical installation if obtaining the maximum duty from a CBE is the only design criterion. However, if an installation that is within 30° of the vertical is desired, a sacrifice of less than 5% of the CBE duty may be acceptable for some applications.

Condenser

Clockwise and counterclockwise rotation tests were performed on the condenser. Vapor superheated to 40 K above the saturation temperature entered the test brazed plate condenser. The superheated vapor was condensed to liquid and subsequently subcooled to approximately 8 K below the saturation temperature.

Figure 9 shows the normalized duty of the condenser as a function of inclination angle (ω). For a given test run, the data were normalized by the duty measured at the vertical position (q_{c0}). The data illustrate that neither rotation nor rotation direction had any effect on the condenser duty. The condenser heat transfer was within 2% of the vertical (0°) value, which was within the u_c of the heat transfer measurement. Recall that the tests were conducted to meet a fixed condensing pressure and entering and leaving refrigerant temperatures. The operating conditions were achieved while the condenser refrigerant mass flow rate remained at approximately 0.029 kg/s for all tests. The ability of the condenser to satisfy the refrigerant state at a fixed refrigerant mass flow implies that it did not experience a heat transfer degradation with rotation.

Figures 10 and 11 show the overall conductance (UA_c) and the composite log-mean temperature

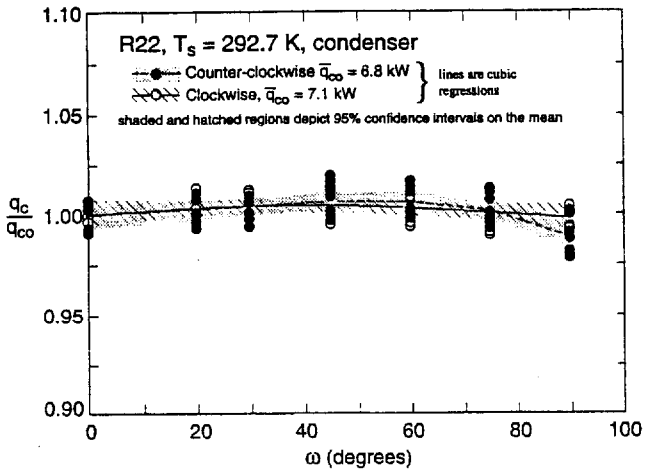

Figure 9 Normalized duty of the condenser as a function of inclination angle.

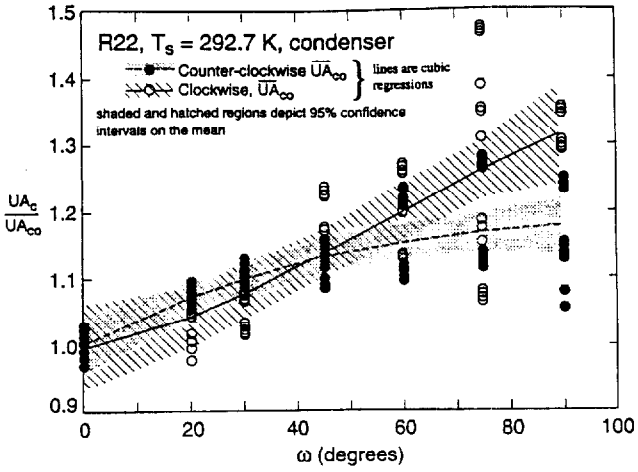

Figure 11 Normalized overall conductance of the condenser as a function of inclination angle.

difference ($\Delta\overline{T}_c$) versus inclination angle (ω). The shaded regions depict the 95% confidence intervals. The figures show that the constant condenser load was met by an increasing UA_c and a decreasing $\Delta\overline{T}_e$. Both the UA_c and the $\Delta\overline{T}_e$ behaved almost linearly with rotation. The difference between counterclockwise and clockwise rotation was within the u_c of the UA_c calculation for rotation angles less than 60°. For angles greater than 60°, the 5–13% difference between the UA_c for the two rotation directions may be due to inadvertent differences in the amount of refrigerant subcooling for the different rotations. More subcooling was achieved for the clockwise rotation (7.1 K) than for the counterclockwise rotation (10.6 K). One consequence of differences in subcooling is shown in Table 5. Table 5 shows that the UA for the condenser rotated clockwise is approximately 25% lower than for the condenser rotated counterclockwise. Differences in subcooling could also be responsible for the differences in the normalized UAs in the horizontal position.

Overall, Figures 10 and 11 show that installation of a CBE condenser in the horizontal position is more favorable for heat transfer than the vertical position. The overall conductance of the condenser in the horizontal position was approximately 17% and 30% greater than that for the vertical position for the counterclockwise and clockwise rotations, respectively. The $\Delta\overline{T}_c$ in the horizontal position was approximately 16% and 23% smaller than that in the vertical position for the counterclockwise and clockwise rotations, respectively. A 20% reduction in $\Delta\overline{T}_c$ typically represented a reduction of less than 2 K.

Figure 12 shows the refrigerant-side, condenser pressure drop (ΔP_c) for refrigerant downflow plotted against the rotation angle. The mean pressure drop remained within 2% of the vertical value for all angles of counterclockwise rotation. Gravitational effects were small because most of the volume (height) in the condenser was in the vapor phase. Conversely, gravity influences the pressure drop for the clockwise rotation past 45°. As shown in Figure 1, the refrigerant exit port is located near the top of the channel. Consequently, refrigerant must accumulate in the channel before exiting. The greater holdup of liquid in the condenser increased the pressure drop of the condenser for the clockwise rotation.

In summary, it is preferable to install the CBE in the horizontal position if maximizing the performance of a condenser is the only goal. There

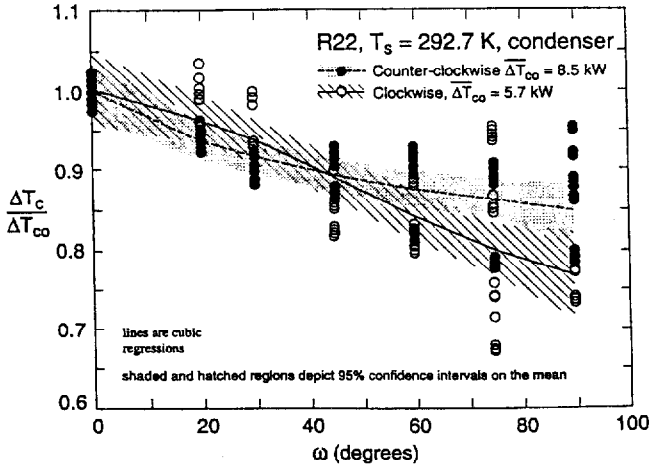

Figure 10 Composite log-mean temperature difference of condenser versus inclination angle.

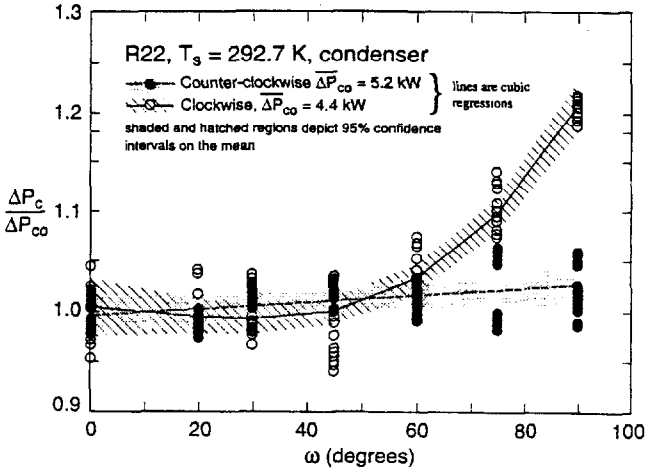

Figure 12 Refrigerant-side pressure drop of condenser versus inclination angle.

may be other design considerations that override concerns for improvement of condenser duty. For example, the condenser of a heat pump during the cooling cycle becomes the evaporator during the heating cycle. Consequently, any performance gained in the horizontal condenser would be more than lost in the horizontal evaporator.

DISCUSSION

Figure 13 shows the hypothesized liquid/vapor distribution within the heat exchanger for the evaporator and the condenser. The cross-sectional flow areas of the channels are simplified for ease of illustration. Nevertheless, the concepts for the overall liquid and vapor distributions should remain valid.

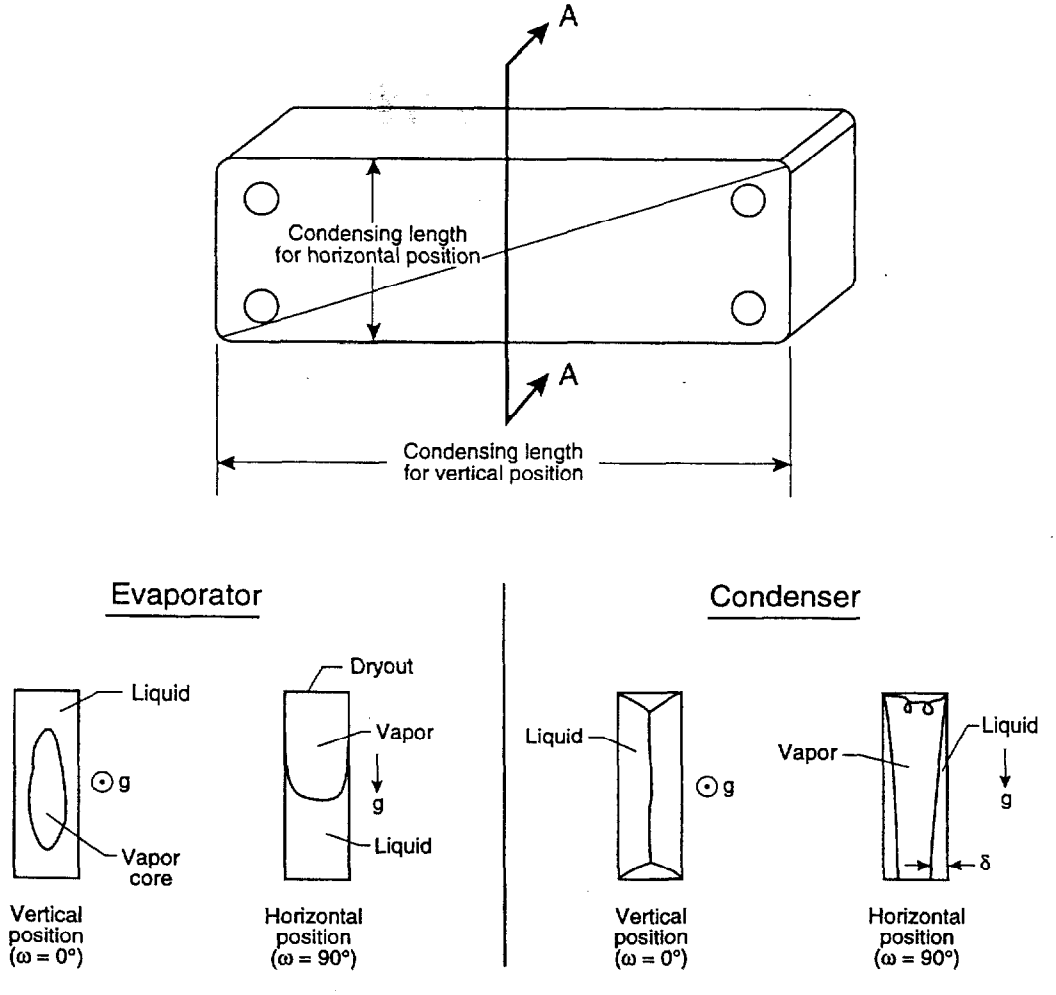

Figure 13 Liquid/vapor distribution within simplified heat exchanger channel for the evaporator and the condenser.

The evaporator suffers a degradation when it is tilted horizontally, due to stratification of the flow. The stratified flow causes dryout of the upper surface of the channel and accumulation of liquid into thick films on the lower portion of the channel. Both dryout and thick liquid films cause poor heat transfer. The vertical position is favorable for flow boiling because the liquid film is distributed more evenly in an annular flow pattern. Consequently, the liquid film is thin and effective for heat transfer in annular flow.

Figure 13 also describes the mechanism responsible for the improvement of the overall heat transfer coefficient of the condenser when it is tilted in the horizontal position. The rotation changes the condensing length of the film. The condensing length is 72 mm and 466 mm long when the condenser is in the horizontal and vertical positions, respectively. The longer condensing length permits the film thickness to build. The thin film region near the leading edge of the condensing length exhibits the most favorable heat transfer. The length of the leading edge for the condenser in the horizontal position is nearly 6.5 times that for the condenser in the vertical position. Consequently, the average condensate film thickness for the condenser in the horizontal position is thinner than that in the vertical position. Thin condensate films induce a greater overall heat transfer coefficient for the condenser in the horizontal position.

CONCLUSIONS

Experimental investigation of the effect of inclination on the performance of a brazed plate heat exchanger revealed that a substantial performance penalty occurs for the evaporator as it is rotated past 30° from the vertical. The evaporator lost 60–75% of its duty to maintain fixed refrigerant states when tilted to the horizontal position, whereas the condenser satisfied fixed refrigerant states without a loss in heat transfer when tilted. The overall heat transfer coefficient of the condenser improved by approximately 17–30% by rotating it to the horizontal position. Consequently, a vertical condenser duty may be improved with a change to a horizontal installation. However, the evaporator should be installed in a vertical or near-vertical position to avoid a significant heat transfer penalty.

Rotation direction and entering-refrigerant state had little effect on the performance of the evaporator for rotation angles less than 60°. For a rotation angle of 30°, the heat transfer degradation was within 5% of the vertical value. The evaporation degradation results from stratification of the flow into a dryout region and a thick film region. Only when the evaporator was rotated to the full horizontal position did rotation direction and refrigerant state have much effect. At the horizontal position, a subcooled-entering refrigerant and a counterclockwise rotation both tended to minimize the heat transfer degradation.

Rotation direction had little effect on the condenser duty. The overall heat transfer coefficient of the condenser improved nearly linearly with rotation. The results suggest that a compact brazed heat exchanger performs best as a condenser when the width is installed in the vertical direction to give the shortest condensing length.

Gravity and flow regime changes both acted to reduce the refrigerant-side pressure drop as the evaporator was rotated from the vertical to the horizontal position. Little change in the pressure drop was observed for a counterclockwise rotation of the condenser. For a clockwise rotation, the condenser pressure drop began to increase past a rotation angle of 60°.

NOMENCLATURE

ccw	counterclockwise
c_p	specific heat (kJ/kg · K)
cw	clockwise
$\dot{m}$	mass flow rate (kg/s)
q	test heat exchanger duty (W)
T	temperature (K)
UA	overall conductance (W/K)
u_c	combined standard uncertainty
ΔP	refrigerant-side pressure drop (kg/m · s^2)
$\Delta \bar{T}$	composite log-mean temperature difference (K)
ω	angle of rotation from the vertical (degrees)

Subscripts

c	condenser
e	evaporator
i	inlet
l	liquid refrigerant
o	outlet
r	refrigerant
v	refrigerant vapor
w	water
w_l	water at saturated refrigerant liquid location

w_v water at saturated refrigerant vapor location
2ϕ two phase refrigerant
0 vertical position

APPENDIX A

This appendix presents the equations that were used to calculate the average temperature difference between the water and the condensing refrigerant vapor (ΔT_v), between the water and the two-phase refrigerant ($\Delta T_{2\phi}$), and between the water and the refrigerant liquid (ΔT_l).

Evaporator

The average temperature between the refrigerant and water streams while the refrigerant was single-phase vapor (ΔT_v) was calculated as

$$\Delta T_v = \frac{(T_{r_o} - T_s)\left[\left(\dot{m}_r c_{p_v}/\dot{m}_w c_{p_w}\right) - 1\right]}{\ln\left[(T_{w_i} - T_{r_o})/(T_{w_v} - T_s)\right]} \tag{3}$$

where $\dot{m}_r$ and $\dot{m}_w$ are the refrigerant and water mass flow rates, respectively. The cp_v and the cp_w are the specific heats of the refrigerant vapor and the water, respectively. The temperature of the water at the location of the saturated refrigerant vapor (T_{w_v}) was calculated from

$$T_{w_v} = T_{w_i} - \frac{\dot{m}_r c_{p_v}}{\dot{m}_w c_{p_w}}(T_{r_o} - T_s) \tag{4}$$

The average temperature difference between the water and the single-phase refrigerant liquid was calculated from

$$\Delta T_l = \frac{(T_{w_l} - T_s) - (T_{w_o} - T_{r_i})}{\ln\left[(T_{w_l} - T_s)/(T_{w_o} - T_{r_i})\right]} \tag{5}$$

where

$$T_{w_l} = T_{w_o} + \frac{\dot{m}_r c_{p_l}}{\dot{m}_w c_{p_w}}(T_s - T_{r_i}) \tag{6}$$

The average temperature difference between the water and the two-phase refrigerant liquid was calculated from

$$\Delta T_{2\phi} = \frac{T_{w_v} - T_{w_l}}{\ln\left[(T_{w_v} - T_s)/T_{w_l} - T_s\right]} \tag{7}$$

Condenser

The average temperature between the refrigerant and water streams while the refrigerant was single-phase vapor (ΔT_v) was calculated as

$$\Delta T_v = \frac{(T_{r_i} - T_s)\left[1 - \left(\dot{m}_r c_{p_v}\right)/\left(\dot{m}_w c_{p_w}\right)\right]}{\ln\left[(T_{r_i} - T_{w_o})/(T_s - T_{w_v})\right]} \tag{8}$$

where $\dot{m}_r$ and $\dot{m}_w$ are the refrigerant and water mass flow rates, respectively. The cp_v and the cp_w are the specific heats of the refrigerant vapor and the water, respectively. The temperature of the water at the location of the saturated refrigerant liquid (T_{w_l}) was calculated from

$$T_{w_v} - T_{w_o} - \frac{\dot{m}_r c_{p_v}}{\dot{m}_w c_{p_w}}(T_{r_i} - T_s) \tag{9}$$

The average temperature difference between the water and the single-phase refrigerant liquid was calculated from

$$\Delta T_l = \frac{(T_s - T_{w_l}) - (T_{r_o} - T_{w_i})}{\ln\left[(T_s - T_{w_l})/(T_{r_o} - T_{w_i})\right]} \tag{10}$$

where

$$T_{w_l} = T_{w_i} + \frac{\dot{m}_r c_{p_l}}{\dot{m}_w c_{p_w}}(T_s - T_{r_o}) \tag{11}$$

The average temperature difference between the water and the two-phase refrigerant liquid was calculated from

$$\Delta T_{2\phi} = \frac{T_{w_l} - T_{w_v}}{\ln\left[(T_s - T_{w_v})/(T_s - T_{w_l})\right]} \tag{12}$$

APPENDIX B

This appendix presents the equations that were used to calculate the vapor, two-phase, and liquid components of heat, q_v, $q_{2\phi}$, and q_l, respectively.

The refrigerant vapor heat load for the condenser was calculated from

$$q_{c_v} = \dot{m}_r c_{p_v}(T_{r_i} - T_s) \tag{13}$$

The refrigerant vapor heat load for the evaporator was calculated from

$$q_{e_v} = \dot{m}_r c_{p_v}(T_s - T_{r_o}) \tag{14}$$

The refrigerant liquid heat load for the condenser was calculated from

$$q_{c_l} = \dot{m}_r c_{p_l}(T_s - T_{r_o}) \tag{15}$$

The refrigerant liquid heat load for the evaporator was calculated from

$$q_{e_l} = \dot{m}_r c_{p_l}(T_{r_i} - T_s) \tag{16}$$

The two-phase refrigerant heat load was calculated from

$$q_{2\phi} = \dot{m}_w c_{p_w}|T_{w_o} - T_{w_i}| - q_v - q_l \tag{17}$$

REFERENCES

[1] Saunders, E. A. D., *Heat Exchangers Selection, Design and Construction*, John Wiley, New York, 1988.

[2] Falls, R. S., Carter, J. R., and Kavanaugh, S. P., Test Results of a Water-to-Air Heat Pump with a Brazed Plate Heat Exchanger for Ground-Coupled Applications, *ASME-JSES-KSES Int. Sol. Energy Conf., Part 1*, pp. 417–423, 1992.

[3] Jonsson, I., Plate Heat Exchangers as Evaporators and Condensers for Refrigerants, *Austral. Ref., Air Cond. Heating*, vol. 39, no. 9, pp. 30–31, 1985.

[4] Saniei, N., and Said, D., Effect of Height and Geometry on Local Heat Transfer and Pressure Drop in a Channel with Corrugated Walls, *Heat Transfer Eng.*, vol. 14, no. 4, pp. 19–31, 1993.

[5] Tinaut, F. V., Melgar, A., and Rahman Ali, A. A., Correlations for Heat Transfer and Flow Friction Characteristics of Compact Plate-Type Heat Exchangers, *Int. J. Heat Mass Transfer*, vol. 35, no. 7, pp. 1659–1665, 1992.

[6] Kumar, H., The Plate Heat Exchanger: Construction and Design, *First U.K. National Conference on Heat Transfer*, vol. 2, pp. 1275–1278, 1984.

[7] Wang, Z., and Zhao, Z., Analysis of Performance of Steam Condensation Heat Transfer and Pressure Drop in Plate Condensers, *Heat Transfer Eng.*, vol. 14, no. 4, pp. 32–41, 1993.

[8] SWEP International. *Compact Brazed Heat Exchangers for Refrigerant Applications*, Technical Handbook, 1992.

[9] Engelhorn, H. R., and Reinhart, A. M., Investigations on Heat Transfer in a Plate Evaporator, *Chem. Eng. Process*, vol. 28, pp. 143–146, 1990.

[10] Edwards, M. F., Ellis, D. I., and Amooie-Foumeny, M., The Flow Distribution in Plate Heat Exchangers, *First U.K. National Conference on Heat Transfer*, vol. 2, pp. 1289–1302, 1984.

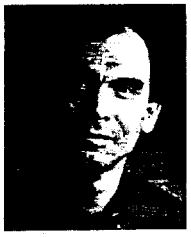

Mark A. Kedzierski is a mechanical engineer at the National Institute of Standards and Technology. He investigates two-phase heat transfer of alternative and multicomponent refrigerants with and without oil both on the fundamental and applied basis. He received his Ph.D. in Mechanical Engineering from The Pennsylvania State University in 1987. Dr. Kedzierski has taught professional short courses on heat transfer enhancement and alternative refrigerants. He also works closely with DuPont, Trane, Wolverine, UOP, and ICI to ensure that his research is of value to these U.S. industries. He was recognized with the William P. Slichter award for his contribution to building and strengthening ties between NIST and industry. Dr. Kedzierski has also received the Bronze Medal award from the Department of Commerce for improving the mechanistic understanding of heat transfer-enhancing additives and refrigerant/lubricant mixtures. Dr. Kedzierski is an associate member of the American Society of Mechanical Engineers. He currently is Chair of the ASME Heat Transfer Division's K-10 Heat Transfer Equipment Committee, and Past Chair of the Government Relations Committee.